KSCE Journal of Civil Engineering (2022) 26(9):3945-3953
DOI 10.1007/s12205-022-1355-z

pISSN 1226-7988, eISSN 1976-3808
www.springer.com/12205

Structural Engineering

Fatigue Resistance of a BFRP-Encapsulated Long-Gauge FBG Strain Sensor under Cyclic Train Loads

Bitao Wu[a], **Yujian Zhou**[b], **Huaxi Lu**[b], **Yun Huang**[b], **and Zhenwei Zhou**[c]

[a]*State Key Laboratory of Performance Monitoring Protecting of Rail Transit Infrastructure, East China Jiaotong University, Nanchang 330013, China*
[b]*School of Civil Engineering, East China Jiaotong University, Nanchang 330013, China*
[c]*School of Civil Engineering, Southeast University, Nanjing 210000, China*

ARTICLE HISTORY

Received 1 August 2021
Revised 18 January 2022
Accepted 20 March 2022
Published Online 1 July 2022

KEYWORDS

Fatigue monitoring
Fiber bragg gratings
Long-gauge FBG sensor
Structural health monitoring
Fatigue resistance

ABSTRACT

To verify the performance of a basalt fiber reinforced polymer (BFRP) fiber-encapsulated long-gauge strain sensor in railway bridge health monitoring, this paper studies the fatigue resistance and durability of the BFRP fiber-encapsulated FBG sensor under train loads. First, the influences of the length of the anchorage section and the length ratio of the sensing section on the accuracy of the sensor were studied. Then, the BFRP sensor was applied to a sleeper for 2 million cycles of tension fatigue testing. The strain-time history of the whole fatigue test was monitored and compared. After the test, a calibration test was carried out to verify the accuracy and repeatability of the sensor. Finally, the slip and fatigue cracking of the fiber in the anchorage section of the sensor were observed by electron microscopy. The results show that the gap between the anchoring section and the bare optical fiber was filled with epoxy resin, and there was no slip behavior. No fatigue cracking occurred in the fiber, and the strain coefficient and linearity of the sensor showed no obvious changes after 2 million cycles of loading. The long-gauge strain sensor encapsulated by BFRP fibers exhibited good fatigue resistance and can meet long-term monitoring requirements under train loads.

1. Introduction

Since the fiber Bragg grating (FBG) sensor was first used for strain measurements in civil engineering in 1992, FBG sensors have been widely used in the health monitoring of civil structures (Prohaska et al., 1993; Górriz et al., 2014; Zhang et al., 2015; Fanelli et al., 2017). Compared with traditional resistive strain sensors, FBG sensors have the advantages of small size, high accuracy, no electromagnetic interference, good corrosion resistance, extensive monitoring objects, good durability, etc. (Moyo et al., 2005; Villalba and Casas, 2013; Wang et al., 2019). However, bare FBG sensors are very fragile and easy to break, so encapsulation is usually required to adapt the sensor to the harsh monitoring conditions of civil engineering applications, common encapsulation materials include metals and fibers (Zhou et al., 2003). A metal package is used for embedded monitoring conditions, and a fiber package is used for external monitoring on the surface of a structure (Saccomandi et al., 2015). BFRP has the advantage of being lightweight and corrosion-resistant. At the same time, the linear expansion coefficient of BFRP is similar to that of concrete, so the relative deformation caused by temperature changes can be reduced, which is beneficial to the monitoring accuracy of the sensor after encapsulation (Tang et al., 2009; Zhou et al., 2016). Therefore, BFRP is an ideal encapsulation material for FBG sensors.

Traditional "point" strain sensors are prone to failure due to minor damage in applications such as bridge damage identification and stiffness evaluation (Calderón and Glisic, 2012). However, a long-gauge FBG (LG-FBG) sensor can overcome the above shortcomings for use in distributed monitoring and has obvious advantages in capturing the structural damage and stress distribution of large-span structures (Glisic, 2011). By installing the BFRP-encapsulated LG-FBG strain sensor at the bottom of a highway bridge, Wu et al. (2016, 2017) successfully proposed a simple-supported beam bridge damage identification method based on the long-gauge strain influence line coefficient and long-gauge

CORRESPONDENCE Bitao Wu wubitao@yeah.net State Key Laboratory of Performance Monitoring Protecting of Rail Transit Infrastructure, East China Jiaotong University, Nanchang 330013, China

stiffness coefficient. Furthermore, this method was extended to continuous beam bridges (Wu et al., 2018). This method can identify the loss of stiffness without interrupting traffic and is not affected by the speed, number of axles, or weight of the vehicle. However, this technique is suitable only for single-vehicle traffic. To overcome the above shortcomings, Chen et al. (2019a, 2019b) further proposed a damage and vehicle load identification method based on the LG-FBG strain sensor and identified the location and degree of damage as well as the vehicle speed, wheelbase, and axle load under multivehicle traffic situations.

The BFRP-encapsulated LG-FBG strain sensor also has good prospects for railway bridge applications. Torres Górriz et al. (2017) compared the accuracy of "point" strain sensors and the long-gauge strain sensor for monitoring railway bridges and demonstrated that the long-gauge sensor can provide accurate measurements. Li (Li and Chen, 2018) evaluated the dynamic and static flexural stiffness of a railway bridge by monitoring the long-gauge strain caused by a maglev train on the bridge and the vibration mode after it quickly crossed the bridge.

Analysis of the above literature shows that BFRP-encapsulated LG-FBG strain sensors have good prospects for applications in bridge health monitoring and are an important research direction for the long-term intelligent monitoring of bridges in the future. However, in the long-term health monitoring of bridges, sensors will need to bear the fatigue load caused by the long-term movement of vehicles. This is especially true for railway bridges, on which the speed and amplitude of trainloads are significantly greater than those on highway bridges. The fiber strength of an FBG sensor under cyclic tensile loading will be reduced due to the stress corrosion effect, leading to subcritical crack growth and thus affecting the integrity of the detection signal (Matthewson and Padiyar, 2001; Gy, 2003). Therefore, the fatigue resistance of the BFRP-encapsulated LG-FBG strain sensor under train loading needs to be further studied.

Mrad and Sparling (Mrad et al., 1999) found that the quality of FBG sensor signals was reduced under tension fatigue loading, but the mechanism responsible for the loss in sensor integrity was not examined. Herszberg et al. (2007) found that the functionality of FBG sensors did not change after one million compression fatigue loads. Ang et al. (2010) evaluated the fatigue properties of chemically or mechanically stripped fiber sensors under cyclic tensile loading. An FBG sensor bonded to the composite substrate was tested in a modified four-point bending rig to test the tensile fatigue properties of FBG sensors. The results showed that the tensile strength of the mechanically stripped fiber was lower than that of the chemically stripped fiber because larger surface flaws were created during the removal of the polymer coating. Frieling and Walther (2013) tested the fatigue properties of three different FBG sensors encapsulated by polyimide, OMF, and PKF. The results showed that under cyclic loading, polyimide fibers endure less strain capability than OMF fibers. Wang and Xiang (2016) proposed a strain transfer mechanism in a three-layer testing model composed of sensing fibers to correct the strain transfer error induced by the shear lag effect and improve the measurement accuracy of FBG sensors under fatigue loading.

Referring to the above literature, the main factors that affect the fatigue performance of the BFRP-encapsulated LG-FBG strain sensor include: 1) whether the fixed connection component experiences slippage and 2) whether the FBG sensor has cracked due to fatigue loading. Increasing the length of the fixed connection component can ensure its anchoring performance but at the same time increases the total length of the sensor; as a result, the excessively long part of the sensor is connected in series, which makes the installation of the sensor inconvenient and affects the sensitivity of the sensor.

For this reason, this article first analyzes and verifies the relationship between the length of the fixed connection component and the sensitivity of the sensor. At the same time, to verify that the sensor can monitor the long-term health of railway bridges, the fatigue resistance and durability of the BFRP-encapsulated LG-FBG strain sensor under trainloads were studied, and the strain time history during the entire fatigue experiment was compared. To verify the reliability of the BFRP-encapsulated LG-FBG strain sensor after 2 million cycles of train loads, a sensor calibration experiment was carried out after the fatigue experiments. Finally, electron microscopy was used to observe whether the fixed connection component of the sensor slipped and whether the FBG had fatigue cracks. The research results show that the gap between the FBG, hollow sleeve, and BFRP sleeve is filled with epoxy resin without slipping; the FBG does not show fatigue microcracks, and the strain coefficient and linearity of the sensor do not change significantly after 2 million cycles of loading.

2. Sensitivity Analysis and Calibration Experiment

2.1 Sensitivity Analysis

The BFRP-encapsulated LG-FBG strain sensor is composed mainly of a fixed connection component and gauge component, as shown in Fig. 1. The bare optical fiber of the gauge component is protected by a hollow sleeve. The diameter of the hollow sleeve is larger than that of the FBG to ensure that the FBG can expand and contract freely in the sleeve. The FBG of the fixed connection is bonded with the hollow sleeve through an epoxy resin. Finally, a BFRP sleeve is used to wrap the fixed connection component and gauge component and the entire BFRP sleeve is infiltrated with epoxy resin to ensure that the sensor has a certain bending stiffness and can be applied mainly to the harsh construction monitoring

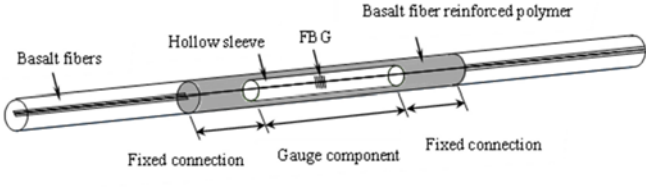

Fig. 1. A Schematic Diagram of the BFRP-Encapsulated LG-FBG Strain Sensor

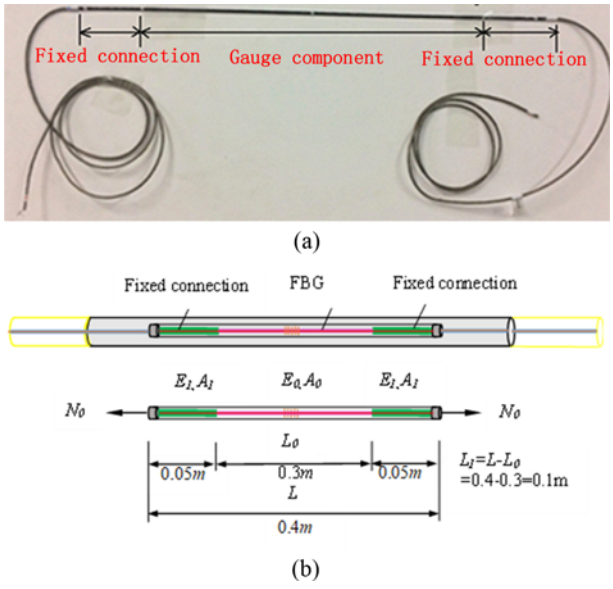

Fig. 2. The LG-FBG Sensor: (a) LG-FBG Sensor Photo, (b) Schematic Diagram

conditions of civil engineering applications.

As shown in Fig. 2, it is assumed that the two ends of the gauge are well bonded to the measured structure and that there is no relative displacement. δ_1 and δ_0 are the displacements of the fixed connection component and the gauge component, respectively. ε_1 and ε_0 are the corresponding strains, and E_1 and E_0 are the corresponding elastic moduli, L and. L_0 are the length of sensor and gauge component, L_1 are the total length of fixed connection.

The total displacement at both ends of the gauge is

$$\delta = \delta_1 + \delta_0 = \varepsilon_1 L_1 + \varepsilon_0 L_0 . \tag{1}$$

Each point in the sleeve is subjected to the same force; therefore,

$$\varepsilon_1 : \varepsilon_0 = \frac{N_0}{E_1 A_1} : \frac{N_0}{E_0 A_0} = \frac{1}{E_1 A_1} : \frac{1}{E_0 A_0} . \tag{2}$$

Therefore, the strain of the FBG component, ε_0, is

$$\varepsilon_0 = \frac{\delta}{L_0 + \frac{E_0 A_0}{E_1 A_1}(L - L_0)} . \tag{3}$$

The average strain $\bar{\varepsilon}$ is

$$\bar{\varepsilon} = \frac{\delta}{L} = \frac{L_0 + \frac{E_0 A_0}{E_1 A_1}(L - L_0)}{L} \varepsilon_0 = ((1 - \frac{E_0 A_0}{E_1 A_1})\frac{L_0}{L} + \frac{E_0 A_0}{E_1 A_1}) \cdot \varepsilon_0 . \tag{4}$$

The simplified form of $\bar{\varepsilon}$ is

$$\bar{\varepsilon} = (\alpha_L + \alpha_E - \alpha_L \alpha_E) \cdot \varepsilon_0 , \tag{5}$$

where $\alpha_E = \frac{E_0 A_0}{E_1 A_1}$, and $\alpha_L = \frac{L_0}{L}$, then, ε_0 can be expressed as

$$\varepsilon_0 = \eta \cdot \bar{\varepsilon}, \tag{6}$$

$$\eta = \frac{1}{\alpha_L + \alpha_E - \alpha_L \alpha_E} , \tag{7}$$

where η is the magnification factor, and the parameters of the LG-FBG sensors in this article are as follows: L_0 = 0.3 m, L_1 = 0.1 m, L = 0.4 m as shown in Fig. 2(b); $A_0 = \pi \times (1252/2)^2$ μm^2, $A_1 = \pi \times (2502/2)^2$ μm^2, E_0 = 5.0 GPa (Ang et al., 2010), and E_1 = 45.0 Gpa (Tang, 2013). Therefore, α_E = 0.443 and α_L = 0.75 can be calculated, and the magnification factor is η = 1.16.

2.2 Calibration Experiment

The calibration experiments with the BFRP-encapsulated LG-FBG sensor were carried out on a calibration table. The experiment consisted of two phases: first, the sensors were slowly pulled, and then the sensors were slowly released. The maximum tensile strain in the test was 3,000 με, and the central wavelength was measured after each deformation of 200 με. To verify the repeatability of the LG-FBG sensor, the calibration experiment was repeated three times, and the average value was taken. The test objects were the LG-FBG1 and LG-FBG2 sensors, which were used to test the fatigue resistance under compression and tension, respectively. The specific tests and results are shown in Fig. 3.

According to Fig. 3(b), the strain coefficients (the ratio of the

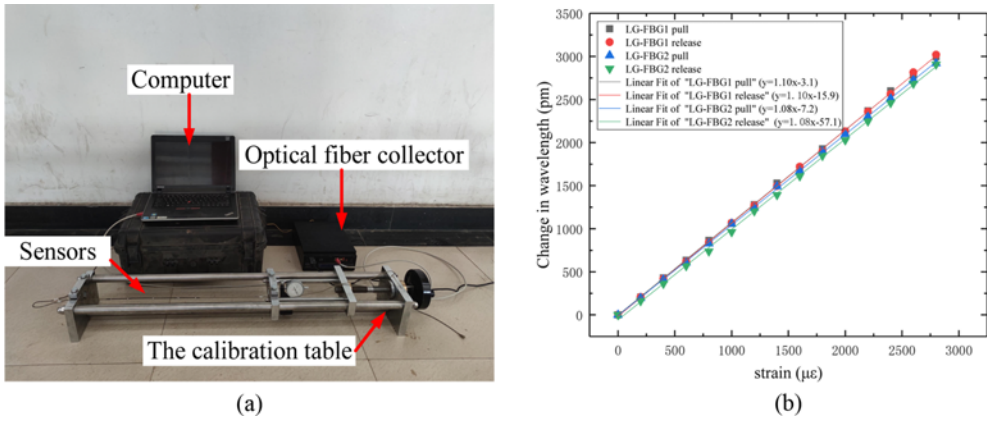

Fig. 3. The Calibration Experiment: (a) The Calibration Table, (b) Experimental Results

change in wavelength to strain) of the LG-FBG1 and LG-FBG2 sensors were 1.10 pm/με and 1.08 pm /με, respectively. The LG-FBG strain sensor with the same BFRP encapsulation has similar calibration coefficients and the advantages of good measurement stability and measurement linearity. For a bare FBG sensor, the ratio of the change in wavelength to strain is approximately 1.0 pm/με, and the strain coefficient and the magnification factor η can be considered to have the same physical significance. Comparing the strain coefficient measured by the test and the magnification factor η calculated by the theory, the error is less than 5%, which confirms the correctness of the above theory.

2.3 Influences of the Fixed Connection Length L_1 and Gauge Length L_0 on the Strain Coefficient

According to the analysis in section 2.1, the length of the fixed connection length L_1 and gauge length L_0 influence the magnification factor η of the sensor. To study these influences, the strain coefficients of the sensors with different L_1 and L_0 are analyzed for a range of fixed connection lengths L_1 = 5 cm – 10 cm and a range of gauge lengths L_0 = 30 cm – 100 cm, and the results are shown in Fig. 4.

Figure 4(a) shows the relationship between the strain coefficient and the fixed connection length L_1. The strain coefficient and L_1 show an obvious linear relationship, the strain coefficient increases linearly with the fixed connection length L_1, and the variation laws of the sensors with different gauge lengths L_0 are the same. Fig. 4(b) shows the relationship between the strain coefficient and the gauge length L_0. According to the analysis of Fig. 4(b), the strain coefficient decreases with increasing gauge length L_0. The strain coefficient for any L_0 and L_1 can be calculated according to the formula in section 2.1.

3. Fatigue Experiment

3.1 Experimental Design

In this fatigue experiment, to truly evaluate the durability performance of the sensors while monitoring railway engineering structures, LG-FBG sensors are pasted on one side of a new type II sleeper, while LG-FBG 1 and LG-FBG2 are located on both sides of the neutral axis to test the fatigue resistance under

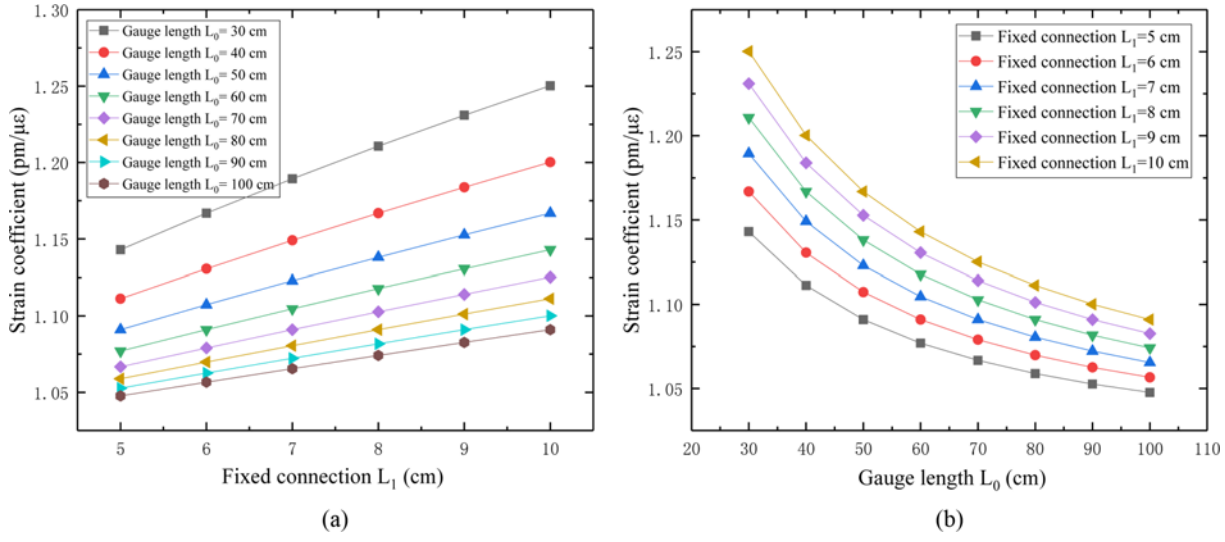

Fig. 4. Relationship between the Strain Coefficient and the Fixed Connection Length L_1: (a) The Relationship between L_1 and the Strain Coefficient, (b) The Relationship between L_0 and the Strain Coefficient

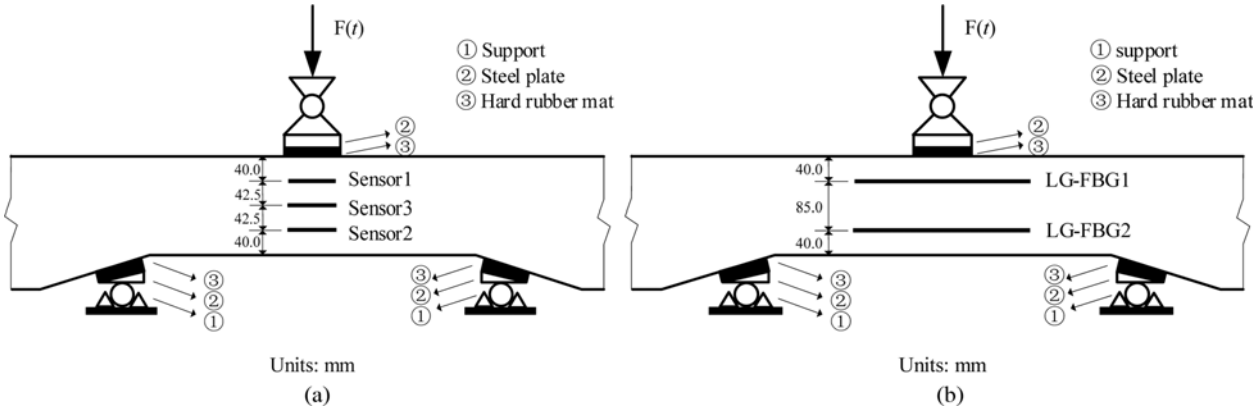

Fig. 5. Schematic Diagram of the Fatigue Experiment Layout: (a) Strain Gauge Layout, (b) Long-Gauge Strain Sensors Layout

Table 1. Main Parameters of the New Type II Sleepers

Parameter	Value	Units
Sleeper length	2500	mm
Concrete strength	C60	MPa
Prestressed steel	8Φ7 or 10Φ6.25	/
Prestress	348	kN
Design bearing bending moment	-12.41	kN.m
Static load anti-crack bending moment	-16.21	kN.m
Maximum load of fatigue experiment	-135	kN

compression and tension, respectively. As a control, the resistive strain sensors are arranged on the other side of the new type II sleeper. The fixed connection component length of all LG-FBG sensors is 5 cm. Due to the long loading time of the fatigue experiment, an LG-FBG strain sensor (LG-FBG3) should be arranged on a concrete block of the same material for temperature compensation. The fatigue experiment arrangement and sleeper parameters are shown in Fig. 5 and Table 1.

According to the relevant regulations of Chinese railways (TB/T1878-2002, 2002), the maximum load of the fatigue experiment is F_{max} = 135 kN, and the cyclic train load cycle characteristic value is $\rho = F_{min}/F_{max} = 0.2$. Therefore, for the cyclic load $F(t) = 54\sin 12\pi t + 81$ adopted in this paper, the maximum and minimum values and frequency of the cyclic train load are 135 kN, 27 kN, and 6 Hz, respectively, and the fatigue times in this paper is determined as 2 million times according to the Fatigue test method for prestressed concrete sleepers (TB/T1878-2002),

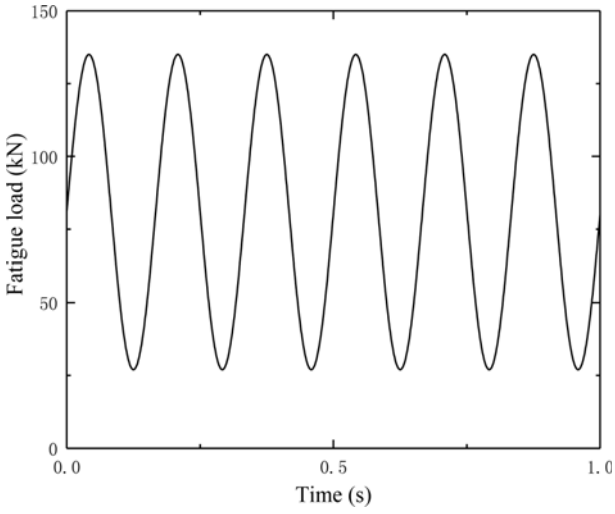

Fig. 6. The Cyclic Train Loads

as shown in Fig. 6. The test was carried out in the Structural Engineering Laboratory of East China Jiaotong University. The experimental machines were three-way fatigue testing machines (GPL-500), located in the structural engineering laboratory of East China Jiaotong University, and an MOI-S155 dynamic optical fiber collector was used to acquire the long-gauge strain.

The installation process of the sensor in the test equipment is shown in Fig. 7, and the details are as follows: 1) The installation position of the sensor is determined, sandpaper is used to polish the surface, and alcohol is used to clean the concrete at the chosen position; 2) The LG-FBG strain sensor is attached to the

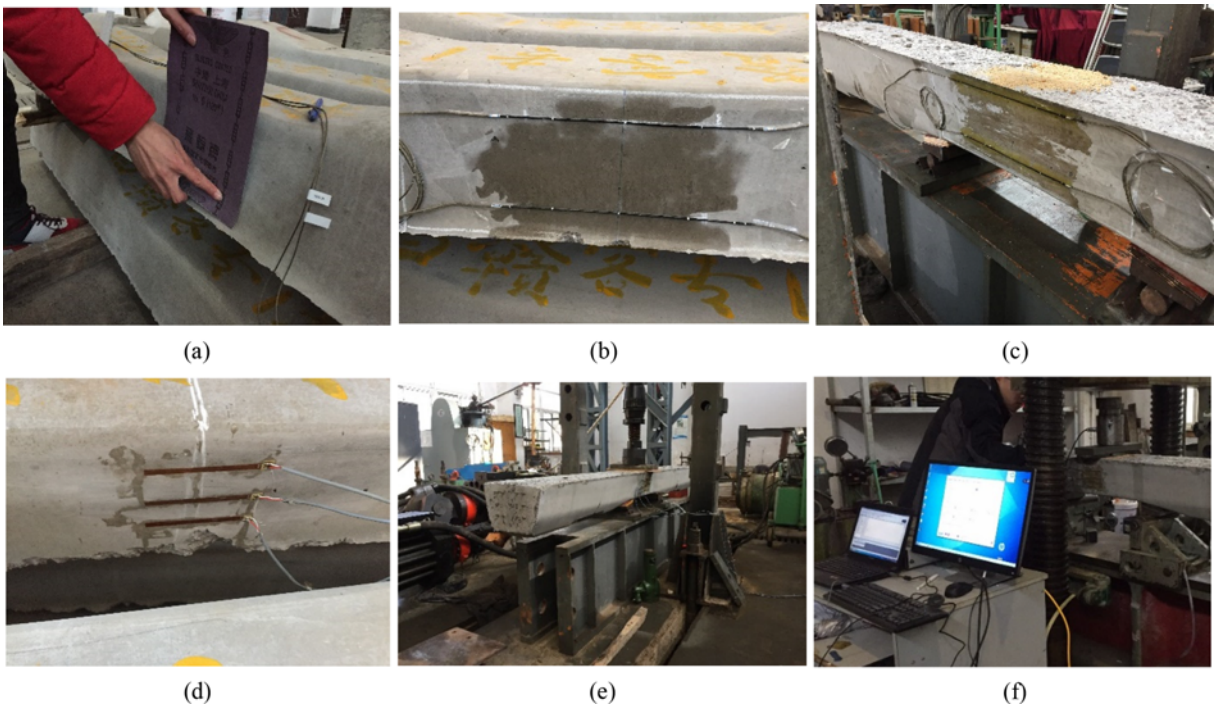

Fig. 7. Fatigue Experiment Process: (a) Sanding The Concrete Surface, (b) Cleaning with Alcohol and Temporarily Fixing the LG-FBG Sensor, (c) Installing the LG-FBG Sensor with Epoxy Resin, (d) Installing the Strain Gauge, (e) Conducting the Fatigue Experiment, (f) Collecting Data

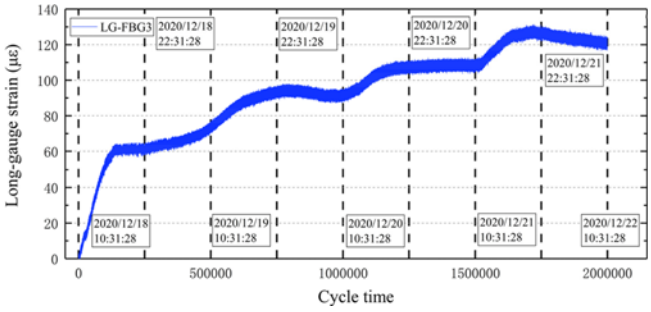

Fig. 8. Long-Gauge Strain Time History Curve of LG-FBG3

concrete surface with epoxy resin to test the compressive and tensile fatigue resistance of the sensor; 3) Three resistive strain sensors are arranged and attached with epoxy resin on the concrete at the corresponding positions on the other side of the sleeper for comparison with the LG-FBG sensor; 4) At the beginning of the test, a preload of 4 kN is applied to eliminate the influence of the bearing gap on the fatigue experiment, and then a cyclic load is applied to the sleeper, and the strain time history during the entire fatigue experiment is monitored by the dynamic optical fiber collector, as shown in Fig. 7.

3.2 Results and Discussions of the Fatigue Experiment

The fatigue experiment lasted 5 days. Fig. 8 shows the strain-time history curve produced by the temperature change of LG-FBG3 during the test. Fig. 8 shows that the temperature change caused the concrete to produce approximately 120 με of strain. During the long-term monitoring process, the indoor temperature increased by 10°C, and the strain caused by the temperature change could not be ignored.

The LG-FBG1 and LG-FBG2 sensors are temperatures compensated by the LG-FBG3 sensor, and the long-gauge strain time-history curves of LG-FBG1 and LG-FBG2 in the fatigue experiment are obtained. To facilitate the comparison with the resistive strain sensor data, the maximum and minimum strains measured by Sensor1 and Sensor2 under cyclic train loads are extracted, as shown in Fig. 9.

Due to a large number of cyclic train loads, the long-gauge strain time history curves of LG-FBG1 and LG-FBG2 cannot show details in Fig. 9(a). For better observation, Fig. 9(b) showed the long-gauge strain time history curves under the cycle of 1000000 to 1000300. Fig. 9 shows that: under the action of cyclic train loads, the long-gauge strains monitored by the sensors LG-FBG1 and LG-FBG2 are in the range of 0 – 410 με and 0 – -300 με, respectively; with an increase in the number of train load cycles, the strain ranges of LG-FBG1 and LG-FBG2 do not change significantly. Compared with the data acquired by the FBG sensors, the strain data monitored by Sensor1 and Sensor2 have the same trend, which verifies that the LG-FBG sensor still has a good monitoring performance after 2 million cyclic train loads. However, the maximum and minimum strain values of Sensor1 and Sensor2 are slightly larger than those of the long-gauge strain monitored by

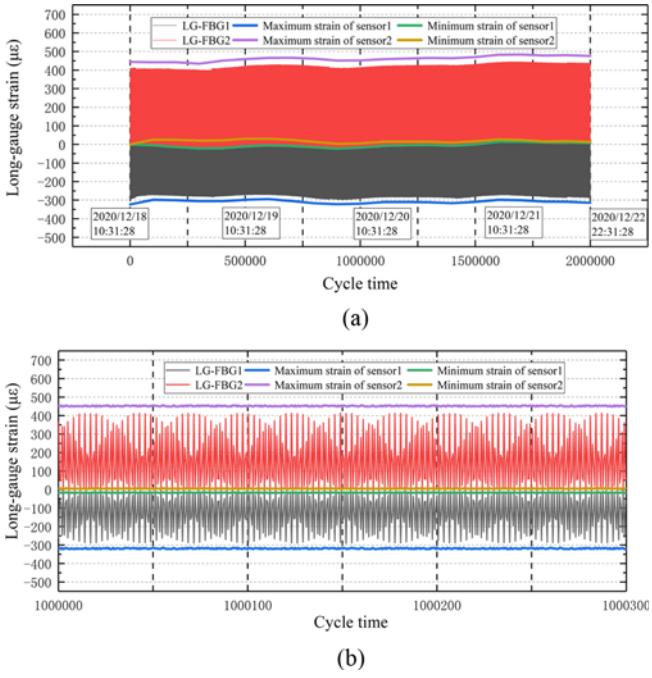

Fig. 9. Long-Gauge Strain Time History under Fatigue Load: (a) Long-Gauge Strain Time-History Curves under 2 Million Cyclic Train Loads, (b) Long-Gauge Strain Time-History Curves between 1,000,000 Cycles and 1,000,300 Cycles

the FBG sensors. This is because the LG-FBG sensors have a larger monitoring range, and the long-gauge strain is the average strain within the monitoring range.

4. Calibration Experiment and Microscopic Observations of the Interfaces after Cyclic Train Loading

4.1 Calibration Experiment after Cyclic Train Loading

To verify the reliability of the BFRP-encapsulated LG-FBG strain sensor after 2 million train loads, a sensor calibration experiment was carried out after the fatigue experiments. The test method is the same as that in section 2.2, and the test results are compared with the test data collected before the fatigue experiment in section 2.2. The results are shown in Fig. 10.

Comparing the data from calibration experiments before and after the fatigue experiment showed that the data points before and after the fatigue experiment coincide. The strain coefficients of tension and release at LG-FBG1 before the fatigue experiment are 1.10 pm/με and 1.10 pm/με, respectively; after the fatigue experiment, they are 1.11 pm/με and 1.10 pm/με, respectively. The strain coefficients of tension and release at LG-FBG2 before and after the fatigue experiment are both 1.08 pm/με. The strain coefficients of the sensors before and after the fatigue experiment are unchanged and have high linearity, which demonstrates that the LG-FBG strain sensor still has good stability after 2 million cyclic train fatigue loads.

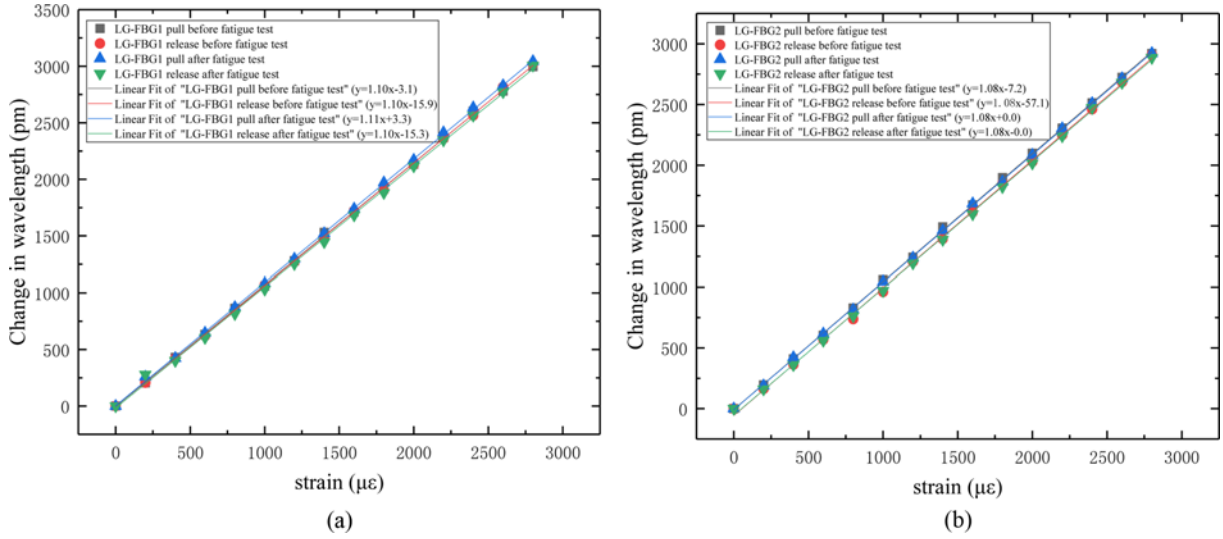

Fig. 10. Comparison of the Calibration Experiments before and after the Fatigue Experiment: (a) Comparison of FBG1, (b) Comparison of FBG2

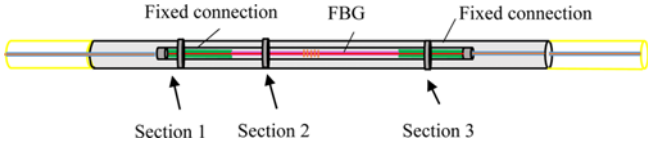

Fig. 11. Positions of the Sensor Sections that Were Observed

4.2 Microscopic Observations of LG-FBG Sensors after Cyclic Train Loading

Based on the monitoring principle of the BFRP-encapsulated LG-FBG strain sensor, the anchoring performance of the fixed connection component determines the service life of the sensor. In the fixed connection component, the FBG is covered by a hollow sleeve, and the gap between the FBG and hollow sleeve must be filled with epoxy resin to ensure the anchoring. The previous section verifies the repeatable performance of the sensor after the 2 million cyclic trainloads from a macroscopic perspective. This section checks whether there are fatigue cracks and voids in the internal structure of the sensor after the fatigue experiment from a microscopic perspective. After the fatigue experiment, the sensor was cut off, and sections of the sensor were observed. As Fig. 11 shows, cuts were made in the two fixed connection sections and the gauge section of the sensor, Section 1 and section 3 are to observe whether the anchorage section slips, and Section 2 is to observe whether the BFRP casing effectively protects the FBG. Figs. 12(a) – 12(c) show an overall cross-sectional view of the fixed connection section, a partially enlarged view of the optical fiber in the fixed connection section, an overall cross-sectional view of the gauge section, and a partially enlarged view of the gauge section casing and the optical fiber.

According to Fig. 12(a), there are three different components of the sensor's fixed connection section: the outer BFRP sleeve, hollow sleeve, and the FBG. The epoxy resin completely covered the gap between the FBG, hollow sleeve, and BFRP sleeve to ensure anchoring. At the same time, the structure of the anchored section is still intact after the fatigue experiment, and there are no gaps or cracks.

In Fig. 12(b), the fiber cross-section of the anchor section shows the rupture caused by the cutting process, but there are no fatigue cracks through the cross-section. There is no slippage between the bare fiber and the hollow sleeve, indicating that the fixed connection section has a good anchoring performance. As shown in Fig. 12(c), the hollow sleeve in the gauge section of the sensor can protect the FBG grating well and ensure the free movement of the FBG so that the sensor is not affected by other external forces. In Figs. 12(d) and 12(e), the bare fiber was pulled out from the protective sleeve. The outermost layer of the protective sleeve is a BFRP sleeve impregnated with epoxy resin, and the inner layer is a hollow sleeve. The BFRP sleeve impregnated with epoxy resin has strong rigidity to ensure the sensitivity of the sensor, and the bare fiber inside the gauge section has a smooth surface without fatigue cracks.

5. Conclusions

In this paper, first, the influences of different fixed connection lengths L_1 and gauge lengths L_0 on the strain coefficient of a BFRP-encapsulated LG-FBG strain sensor are analyzed. Then, the monitoring accuracy of the long-scale strain sensor under 2 million cycles of train loading is verified by a fatigue experiment. After the fatigue experiment, the linearity of the sensor is tested, and the microscopic interface of the sensor is observed by electron microscopy. The main conclusions are as follows:

1. The strain coefficient and L_1 show an obvious linear relationship, the strain coefficient increases linearly with the fixed connection length L_1, and the variation laws of sensors with different gauge lengths L_0 are the same. The strain coefficient decreases with increasing gauge length L_0.
2. The BFRP-encapsulated LG-FBG strain sensor can stably monitor the whole fatigue experiment process. The strain

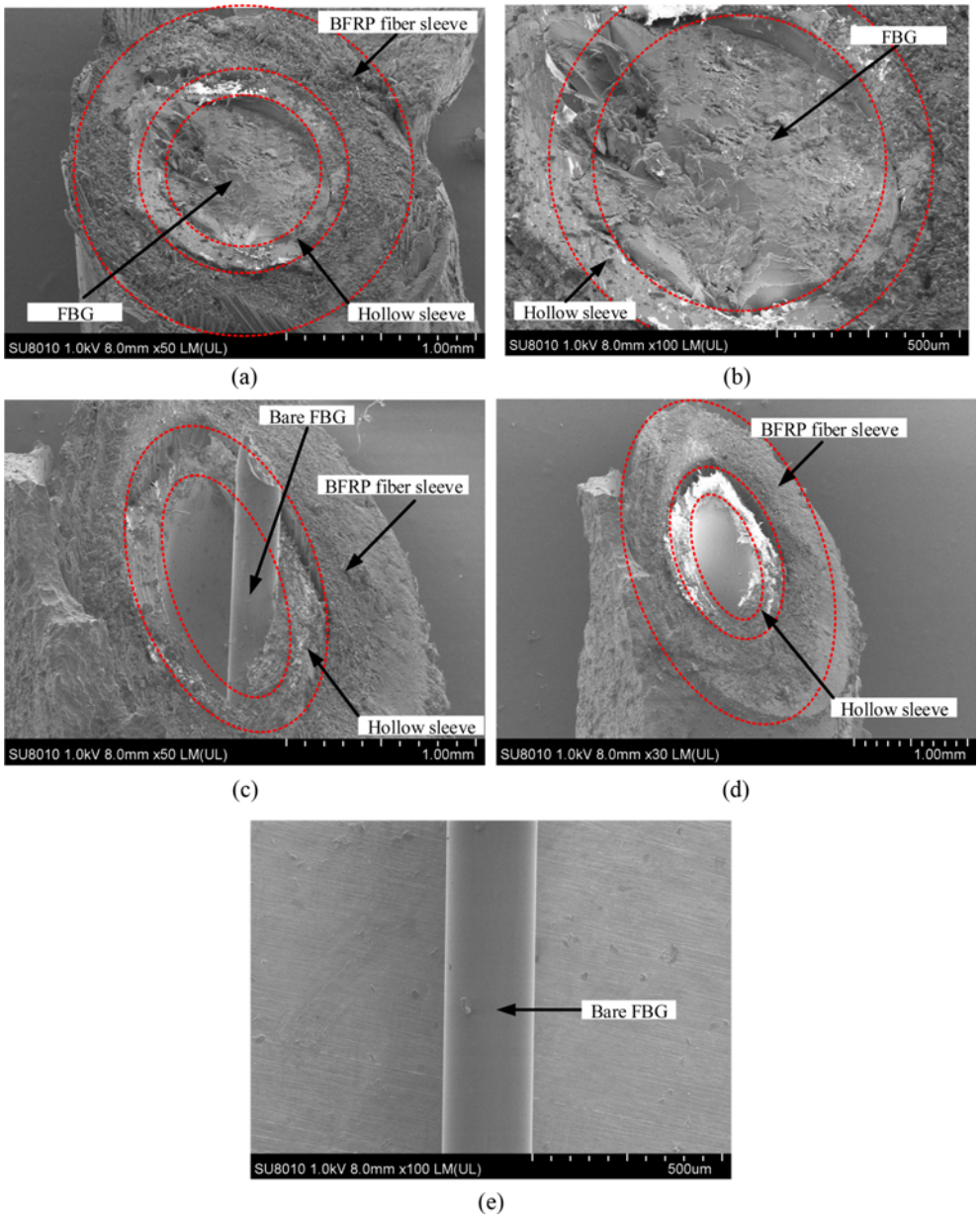

Fig. 12. Electron Microscopy Images of the FBG Sensor: (a) Overall Cross-Sectional View of Section1, (b) Overall Cross-Sectional View of Section 3, (c) Overall Cross-Sectional View of Section2, (d) The BFRP Fiber Sleeve and Hollow Sleeve in Section 2, (e) Bare FBG in Section 2

caused by variation in the ambient temperature during the monitoring process cannot be ignored. When the temperature increases by 1°C, the strain increases by approximately 12 με.

3. After the fatigue experiment, the strain coefficient and linearity of the BFRP-encapsulated LG-FBG strain sensors do not change, which confirms that the sensor still has a good monitoring accuracy even after 2 million cycles of train loading.
4. After the fatigue experiment, the sensor section and gauge section are observed by electron microscopy. The epoxy resin completely covers the gap among the FBG, hollow sleeve, and BFRP sleeve to ensure anchoring. There is no slip between the fiber and the hollow sleeve in the fixed connection section, and there are no fatigue microcracks on the fiber surface or cross-section. In general, when the length of the fixed connection is greater than 5 cm, the BFRP-encapsulated LG-FBG strain sensor can monitor a railway bridge.

Acknowledgments

This paper is supported by the National Natural Science Foundation of China (Grant No. 51808219), Natural Science Foundation of Jiangxi Province (Grant No. 20202BAB214024, 20212BAB204010), and China Postdoctoral Foundation (Grant No. 2018M640607).

ORCID

Bitao Wu https://orcid.org/0000-0002-5193-6525
Yujian Zhou https://orcid.org/0000-0002-5761-8771
Huaxi Lu https://orcid.org/0000-0003-3970-6441
Yun Huang https://orcid.org/0000-0001-9037-2147
Zhenwei Zhou https://orcid.org/0000-0002-1940-2697

References

Ang J, Li H, Herszberg I, Bannister M, Mouritz A (2010) Tensile fatigue properties of fibre Bragg grating optical fibre sensors. *International Journal of Fatigue* 32(4):762-768, DOI: 10.1016/j.ijfatigue.2009.11.002

Calderón PA, Glisic B (2012) Influence of mechanical and geometrical properties of embedded long-gauge strain sensors on the accuracy of strain measurement. *Measurement Science Technology* 23(6):065604, DOI: 10.1088/0957-0233/23/6/065604

Chen S-Z, Wu G, Feng D-C (2019a) Damage detection of highway bridges based on long-gauge strain response under stochastic traffic flow. *Mechanical Systems Signal Processing* 127:551-572, DOI: 10.1016/j.ymssp.2019.03.022

Chen S-Z, Wu G, Feng D-C (2019b) Development of a bridge weigh-in-motion method considering the presence of multiple vehicles. *Engineering Structures* 191:724-739, DOI: 10.1016/j.engstruct.2019.04.095

Fanelli P, Biscarini C, Jannelli E, Ubertini F, Ubertini S (2017) Structural health monitoring of cylindrical bodies under impulsive hydrodynamic loading by distributed FBG strain measurements. *Measurement Science and Technology* 28(2):024006, DOI: 10.1088/1361-6501/aa4eac

Frieling G, Walther F (2013) Tensile and fatigue properties of fiber-bragg-grating (FBG) sensors. *Sensors & Transducers* 154(7):143-148

Glisic B (2011) Influence of the gauge length on the accuracy of long-gauge sensors employed in monitoring of prismatic beams. *Measurement Science Technology* 22(3):035206, DOI: 10.1088/0957-0233/22/3/035206

Górriz BT, García PC, Payá-Zaforteza IJ, Maicas SS (2014) Experimental and numerical analysis of a hybrid FBG long gauge sensor for structural health monitoring. *Measurement Science and Technology* 25(12):125107, DOI: 10.1088/0957-0233/25/12/125107

Gy R (2003) Stress corrosion of silicate glass: A review. *Journal of Non-Crystalline Solids* 316(1):1-11, DOI: 10.1016/s0022-3093(02)01931-2

Herszberg I, Bannister M, Li H, Qi B, Marsden J (2007) Durability under fatigue loading of optical fibres applied to fibre reinforced plastic composites. *The International Society for Optical Engineering* 6619, DOI: 10.1117/12.738395

Li S, Chen S (2018) Structural health monitoring of maglev guideway PC girders with distributed long-gauge FBG sensors. *Structural Control and Health Monitoring* 25(1):e2046, DOI: 10.1002/stc.2046

Matthewson MJ, Padiyar V (2001) Cyclic fatigue of high-strength optical fibers in bending. *International Society for Optics and Photonics* 53-59, DOI: 10.1117/12.424383

Moyo P, Brownjohn J, Suresh R, Tjin S (2005) Development of fiber Bragg grating sensors for monitoring civil infrastructure. *Engineering Structures* 27(12):1828-1834, DOI: 10.1016/j.engstruct.2005.04.023

Mrad N, Sparling S, Laliberte J (1999) Strain monitoring and fatigue life of Bragg grating fiber optic sensors. *The International Society for Optical Engineering* 3670:82-91, DOI: 10.1117/12.349717

Prohaska JD, Snitzer E, Chen B, Maher MH, Nawy E, Morey WW (1993) Fiber optic Bragg grating strain sensor in large-scale concrete structures. *The International Society for Optical Engineering* 1798(1798):286-294, DOI: 10.1117/12.141330

Saccomandi P, Oddo CM, Zollo L, Formica D, Romeo RA, Massaroni C, Caponero MA, Vitiello N, Guglielmelli E, Silvestri S (2015) Feedforward neural network for force coding of an MRI-compatible tactile sensor array based on fiber Bragg grating. *Journal of Sensors* 2015, DOI: 10.1155/2015/367194

Tang Y (2013) Research on structural intelligence based on distributed optical fiber sensing and self-sensing FRP. PhD Thesis, Southeast University, Nanjing, China, DOI: 10.7666/d.Y2511461

Tang Y, Wu Z, Yang C, Shen S, Wu G, Hong W (2009) Development of self-sensing BFRP bars with distributed optic fiber sensors, smart sensor phenomena, technology, networks, and systems 2009. *International Society for Optics and Photonics* 729317, DOI: 10.1117/12.815767

TB/T 1878-2002 (2002) Fatigue test method for prestressed concrete sleepers. TB/T 1878-2002, Ministry of Railways of the people's Republic of China, Beijing, China

Torres Górriz B, Rinaudo P, Calderón García PA (2017) Comparison between point and long-gage FBG-based strain sensors during a railway bridge load test. *Strain* 53(4):e12230, DOI: 10.1111/str.12230

Villalba S, Casas JR (2013) Application of optical fiber distributed sensing to health monitoring of concrete structures. *Mechanical Systems Signal Processing* 39(1-2):441-451, DOI: 10.1016/j.ymssp.2012.01.027

Wang H, Xiang P, Jiang L (2019) Strain transfer theory of industrialized optical fiber-based sensors in civil engineering: A review on measurement accuracy, design and calibration. *Sensors Actuators A: Physical* 285:414-426, DOI: 10.1016/j.sna.2018.11.019

Wang H, Xiang P, Li X (2016) Theoretical analysis on strain transfer error of FBG sensors attached on steel structures subjected to fatigue load. *Strain* 52(6):522-530, DOI: 10.1111/str.12195

Wu B, Wu G, Lu H, Feng D-C (2017) Stiffness monitoring and damage assessment of bridges under moving vehicular loads using spatially-distributed optical fiber sensors. *Smart Materials Structures* 26(3):035058, DOI: 10.1088/1361-665x/aa5c6f

Wu B, Wu G, Yang C, He Y (2016) Damage identification and bearing capacity evaluation of bridges based on distributed long-gauge strain envelope line under moving vehicle loads. *Journal of Intelligent Material Systems Structures* 27(17):2344-2358, DOI: 10.1177/1045389x16629571

Wu B, Wu G, Yang C, He Y (2018) Damage identification method for continuous girder bridges based on spatially-distributed long-gauge strain sensing under moving loads. *Mechanical Systems Signal Processing* 104:415-435, DOI: 10.1016/j.ymssp.2017.10.040

Zhang J, Guo S, Wu Z, Zhang Q (2015) Structural identification and damage detection through long-gauge strain measurements. *Engineering Structures* 99:173-183, DOI: 10.1016/j.engstruct.2015.04.024

Zhou Z, Graver TW, Hsu L, Ou JP (2003) Techniques of advanced FBG sensors: Fabrication, demodulation, encapsulation and their application in the structural health monitoring of bridges. *Pacific Science Review* 5(1):116-121

Zhou Z, Wang Z, Shao L (2016) Fiber-reinforced polymer-packaged optical fiber Bragg grating strain sensors for infrastructures under harsh environment. *Journal of Sensors*, DOI: 10.1155/2016/3953750